Skeletal Muscle Proteostasis Promotes Central Nervous System Rejuvenation and Reduces Neuroinflammation during Aging and Neurodegenerative Disease

Ian Matthews [1]

Allison Birnbaum [1]

Anastasia Gromova [2,3]

Kristen Coutinho [1]

Megan McGraw [1]

Dalton Patterson [1]

Macy T. Banks [1]

Amber Nobles [1]

Helen C. Miranda [9]

Albert R. La Spada* [3,10]

Constanza J. Cortes* [1,4-8]

**co-corresponding authors*

[1] Department of Cell, Developmental and Integrative Biology, [2] Biomedical Sciences Graduate Program, University of California, San Diego [3] Department of Pathology and Laboratory Medicine, University of California, Irvine [4] UAB Center for Exercise Medicine, [5] UAB Nathan Shock Center, [6] UAB Alzheimer's Disease Center, [7] UAB Center for Neurodegeneration and Experimental Therapeutics, [8] University of Alabama at Birmingham, [9] Department of Genetics and Genome Sciences, School of Medicine, Case Western University, [10] Department of Neurology and Department of Biological Chemistry, Institute for Neurotherapeutics, University of California, Irvine

Funding: NIH RF1 AG057264 (CJC and ALS), NIH R03 AG063215 (CJC), University of Washington Nathan Shock Center Pilot Grant (CJC)

Acknowledgements: we thank members of the lab past and present for their helpful contributions

ABSTRACT

Skeletal muscle has recently arisen as a novel regulators of Central Nervous System (CNS) function and aging, secreting bioactive molecules known as myokines with proteostasis and metabolism-modifying functions in targeted tissues, including the CNS. Here we report the generation of a novel transgenic mouse with enhanced muscle proteostasis via moderate overexpression of TFEB. We have discovered that the resulting enhanced skeletal muscle proteostasis function can significantly ameliorate proteotoxicity, reduce neuroinflammation and promotes transcriptional remodeling of the aging CNS, preserving cognition/memory in aging mice. Enhancing skeletal muscle proteostasis also reduced neuroinflammation and accumulation of tau-associated pathological hallmarks in a mouse model of tau pathology and was accompanied by increased secretion of CNS-targeting circulating factors from skeletal muscle. Our results implicate maintenance of skeletal muscle proteostasis throughout aging to direct regulations of the aging CNS metabolism and function, and suggest that skeletal-muscle originating factors may act as novel therapeutic targets against age-associated neurodegenerative diseases.

INTRODUCTION

Aging is associated with an organism-wide progressive loss of tissue form and function, broadly characterized by the 'hallmarks of aging'[1]. In particular, the aging central nervous system (CNS)[1,2] exhibits a global loss in protein homeostasis (proteostasis), impaired neuroplasticity and resilience, and an increase in neuroinflammation[2,3]. These alterations are believed to render the aging CNS vulnerable to age-associated dysfunction and the development of neurodegenerative disease[2]. Macroautophagy (hereafter referred to as autophagy) is a central player in proteostasis function, which degrades and recycles intracellular components too large to be processed through the proteasome. Autophagy activity steadily declines with age[4], leading to a chronic accumulation of damaged macromolecules and organelles in aging tissues[4] and contributing to the onset of age-associated diseases[1,4]. In concordance with this, genetic disruption of autophagy in specific cell types is sufficient to drive cellular and biochemical hallmarks of aging in young tissues, including accumulation of protein aggregates[5,6], mitochondrial dysfunction[7] and compromised metabolic signaling[7-9]. Autophagy dysfunction has thus been proposed to act as a primary regulator of biological aging[1,4]. Consistent with this hypothesis, many well-known geroprotective interventions appear to work through the promotion of autophagy function[4]. Indeed, studies have shown that maintenance of global autophagy via genetic[10-12], behavioral[13] and pharmacological[14,15] manipulation extends lifespan in murine and primate models. Autophagy activation *in vivo* also delays the development of age-associated metabolic phenotypes[7,13,16] and preserves motor function during aging[11]. Taken together, these results position autophagy as an excellent target for therapeutic development to prevent age-associated CNS functional decline.

Elegant genetic studies on non-vertebrate models have recently revealed the existence of transcriptional protein quality control feedback between tissues, i.e. the cell-non autonomous control of organismal proteostasis[17-21]. In particular, manipulation of skeletal muscle protein quality control pathways yields important benefits on the CNS by activating proteostasis and protecting against the accumulation of aggregation-prone neurodegenerative disease proteins in the brain and the retina[18,21,22]. Although the mechanisms responsible for these benefits remain poorly understood, some of these effects are mediated by secreted factors that move through the circulation[18,20,22]. Indeed, increasing evidence implicates circulating factors in the blood as potent regulators of mammalian CNS aging and metabolism[23-26]. For example, exposure to a young plasma environment (either through heterochronic parabiosis or plasma transfers) can

rescue function in the aging CNS[25,27] by decreasing neuroinflammation[28] and enhancing neurogenesis[23]. Studies have further demonstrated that increasing the circulating levels of these individual factors in peripheral circulation is sufficient to rejuvenate the aged CNS[25,29,30], supporting the existence of 'pro-youth' circulating factors with CNS targeting effects. Although the source and identity of these neuroprotective circulating cytokines is unclear, several of them are expressed in, and can be secreted from, skeletal muscle[18,31-33]. Accounting for 40% of total body mass, skeletal muscle acts as an endocrine organ secreting a myriad of bioactive factors collectively known as myokines that induce metabolic changes in distant tissues like liver[34], adipose tissue[35] and more recently, the CNS[32]. Interestingly, skeletal muscle function has also arisen as a key predictor for phenotypic and clinical outcomes in age-associated neurodegenerative disease[36,37]. Thus, this muscle-to-brain signaling axis has been proposed to have important implications for CNS aging and age-associated neurodegenerative disease[32,38,39]. Consistent with this hypothesis, we were the first to uncover a novel mechanistic basis for motor neuron disease in the polyglutamine disease spinal and bulbar muscular atrophy (SBMA), where disruption of skeletal muscle autophagy[40] initiates the pathogenic cascade that culminates in neuronal toxicity and death[41,42]. Altogether, this suggests that direct manipulation of skeletal muscle proteostasis may promote neurotrophic signaling in the aging brain, and thus provide positive systemic benefits against age-associated CNS decline.

Skeletal muscle autophagy is regulated in part by the basic Helix Loop Transcription Factor E-B (TFEB), a master regulator of a novel signaling axis that integrates cellular metabolism and autophagy[43-45]. TFEB expression and function is strongly induced in skeletal muscle during low nutrient conditions[16] and after exercise[7], suggesting that TFEB signaling is engaged in skeletal muscle in response to behavioral interventions with documented neuroprotective effects on the aging[46,47] and neurodegenerative disease-afflicted CNS[47-50]. Here we report the generation of a novel transgenic mouse with enhanced muscle proteostasis via moderate overexpression of TFEB. We have discovered that the resulting enhanced skeletal muscle proteostasis function can significantly ameliorate proteotoxicity, reduce neuroinflammation and promotes transcriptional remodeling of the aging CNS, preserving cognition/memory in aging mice. Enhancing skeletal muscle proteostasis also reduced neuroinflammation and accumulation of tau-associated pathological hallmarks in a mouse model of tau pathology and was accompanied by increased secretion of CNS-targeting circulating factors from skeletal muscle. Our results implicate maintenance of skeletal muscle proteostasis throughout aging to direct regulations of the aging CNS metabolism and function, and suggest that skeletal-muscle originating factors may act as novel therapeutic targets against age-associated neurodegenerative diseases.

RESULTS

Generation and validation of muscle-specific TFEB overexpressing mice.

We derived a novel line of conditional transgenic mice carrying the β-actin promoter in combination with the CMV enhancer (CAGGS) and with a floxed 3x-FLAG-eGFP STOP cassette placed just 5' to a 3x-FLAG-human TFEB transgene ("fxSTOPTFEB" mice), allowing for tissue-specific expression of TFEB in the presence of Cre-recombinase (**Figure 1A**). To drive expression of the TFEB transgene specifically in skeletal muscle, we crossed fxSTOP-TFEB mice with Human Skeletal Actin (HSA)-Cre mice to achieve widespread expression of Cre-recombinase in cells of the myogenic lineage[51]. The resulting cTFEB:HSACre bigenic mice exhibited muscle-specific expression of TFEB expression at ~2.5x endogenous levels (**Figure 1B**), with the expected induction of endogenous mouse TFEB caused by the positive feedback loop TFEB auto-regulation[16]. We confirmed myonuclear expression of TFEB in cTFEB:HSA-Cre muscle by immunohistochemistry, which revealed FLAG immunostaining in the myofiber periphery (**Figure 1C**). As expected, we did not detect expression of 3xFlag-TFEB protein in tissues of nonmyogenic origin, including brain (**Figure 3A**).

TFEB overexpression enhances proteostasis and preserves muscle integrity in aging skeletal muscle.

We next confirmed functional activation of the CLEAR network in cTFEB:HSA-Cre bigenic muscle, using our previously reported TFEB-responsive muscle gene targets[40], including Atg5 (a key protein driving autophagy initiation), Cathepsin D (a lysosomal protease) and LAMP1 (an essential lysosomal structural protein) (**Figure 1D**). Consistent with our transcriptional studies, we also detected significant increases of TFEB targets with high relevance on lysosomal function and biology at the protein level, including LAMP1 and cathepsin D (**Figure 1E**). These findings confirm physiologically significant increases in TFEB-mediated transcription in skeletal muscle of cTFEB:HSA-Cre mice.

TFEB transcriptional regulation positively modulates lysosomal function and autophagy[43,45], reactivating declining proteostasis associated with impaired lysosomal function, including in aged tissues[40,52,53]. When we examined levels of the autophagy marker LC3, which is cleaved and post-translationally modified into its mature form (LC3-II) upon autophagy induction[54], we observed a significant increase in LC3-II:LC3-I ratio in quadriceps muscle of 12 month-old

cTFEB:HSA-Cre mice, indicating increased numbers of autophagosomes (**Figure 1F**).One approach to examine this age-associated decline in proteostasis is the examination of poly-ubiquitinated and p62-labeled aggregates, usually representing cytoplasmic accumulations of damaged proteins[4]. Consistent with previous reports of aging skeletal muscle[21], we detected a marked accumulation of p62/SQSTM1 and ubiquitin positive aggregates of varying size in middle-aged (12 months old) control skeletal muscle (**Figure 1G, top**), indicating a progressive increase in protein damage and a decrease in the turnover of skeletal muscle proteins [1,21,55]. Strikingly, these features were nearly absent in skeletal muscle sections from age- and littermate-matched cTFEB:HSA-Cre mice (**Figure 1G, bottom**). We also detected reduced expression of muscle stress factor myostatin in aging cTFEB;HSACre skeletal muscle (**Figure 1H**). Our results thus suggest a maintenance of functional proteostasis in aging skeletal muscle via TFEB overexpression, consistent with previous reports of skeletal muscle induction of TFEB-activity via adenoviral strategies[7,53].

Proteomics Analysis Identifies Increased Proteostasis Related and Metabolism-Associated Proteins in TFEB-Overexpressing Skeletal Muscle.

To examine the changes in the skeletal muscle protein landscape in response to TFEB overexpression, we performed proteome profiling of young (6-month-old) and aged (18-month-old) control and cTFEB;HSACre quadriceps skeletal muscle. Differential abundance analysis of species revealed over ~900 proteins associated with muscle TFEB over-expression (**Figure 2A-B**). Of these, 650 proteins were increased and 350 proteins were decreased in cTFEB;HSACre vs. control skeletal muscle. At both ages examined, TFEB was among the top 5 most highly expressed proteins (**Figure 2A-B, purple rectangles**), confirming maintenance of skeletal muscle TFEB overexpression across ages. KEGG enrichment analysis of overexpressed proteins revealed multiple central proteostasis categories heavily overrepresented in TFEB-overexpressing skeletal muscle, including as Hypoxia-inducible factor 1 (HIF-1) signaling (such as hexokinase 2, Pyruvate Dehydrogenase, Ribosomal Protein S6 Kinase B2, Lactate Dehydrogenase B, for example) and proteasome and autophagy/lysosomal function categories (including cathepsin B, D and K, mTOR, Bnip3 and Lamp1) (**Figure 2C, pink**), consistent with our immunoblot studies (**Figure 1, E-F**). Additional functional categories altered related to cellular metabolism and mitochondrial function, including thermogenesis, oxidative phosphorylation and fatty acid metabolism (**Figure 2C, green**). Interestingly, several signaling pathways shown to decline during aging, including Insulin-IGF1-Signaling and AMPK Signaling[1], were significantly enriched in cTFEB;HSACre transgenic muscle (**Figure 2C, blue**). Finally, we

also detected multiple hits for amino acid metabolism pathways, including catabolism of branched-chain amino acids (valine, leucine, isoleucine, BCAAs), which have been recently linked to lifespan and healthspan extension in rodents[56] (**Figure 2C, purple**). Most of these changes were maintained in our aged cohorts (**Figure 2C, right**). To visualize the key networks of proteins associated with TFEB-overexpression, we performed a functional enrichment analysis on all overexpressed proteins using the STRING protein-protein interaction network[57](**Figure 2D**). Using TFEB as our 'bait' for functional connectivity nodes, we identified two clear interaction networks: one associated with lysosomal biogenesis and function (in blue) and a second one associated with key skeletal muscle proteostasis and metabolic signaling pathways, including mTOR, Akt and GSK3beta (in green). Both of these nodes are key elements of the CLEAR signaling network controlled by TFEB-mediated transcription[44,45], were previously reported to be transcriptionally elevated in skeletal muscle after TFEB overexpression[7], and are central regulators of age-associated signaling[1]. Overall, our results suggests that mild overexpression of TFEB in skeletal muscle throughout the lifespan promotes activation of multiple geroprotective effects on the hallmarks of aging, including mitochondrial function, proteostasis regulation and insulin/IGF1 signaling.

To directly examine any changes to the skeletal muscle 'secretome', we pursued additional *in silico* analysis to identify unique age- and genotype-associated signatures of potentially secreted proteins[58] enriched in cTFEB;HSACre skeletal muscle (**Figure 2E**). Importantly, cathepsin B, a previously documented myokine with known CNS-targeting effects and a known target of TFEB-dependent transcription[33] was our top hit, remaining upregulated at both ages examined. We also identified multiple additional potentially secreted factors enriched at both ages in cTFEB;HSACre-expressing muscle (including prosaposin and mammalian ependymin-related protein 1 and dehydrogenase/ reductase SDR family member 7C). Other factors exhibited upregulation only in young cTFEB;HSACre muscle (e.g., nucleobindin-1, angiopoietin-related protein 1), highlighting the dynamic nature of the skeletal muscle secretion profile throughout aging. We validated the predicted increase in cathepsin B by both transcript (**Figure 2**) and protein analysis (**Figure 2F**) in a separate cohort of cTFEB;HSACre mice, which revealed that this increase is driven by a large increase in mature (secreted) cathepsin B isoforms. We also confirmed significantly increased levels of circulating cathepsin B in the serum of female cTFEB;HSACre mice (**Figure 2G**). Taken together, our data suggests that overexpression of TFEB in skeletal muscle drives increased expression and secretion of cathepsin B into circulation.

Skeletal Muscle Over-expression of TFEB decreases glia activation, neuroinflammation and lipofuscin accumulation in the aged CNS.

One of the key drivers of age-associated cognitive decline is neuroinflammation[2], the chronic activation of glial cells towards pro-inflammatory phenotypes in the CNS. To examine the effect of increased peripheral proteostasis on the aging brain, we assessed the transcriptional and functional status of known inflammatory markers in the CNS of aged mice (20+ months), an age when global decreases in proteostasis and increases in pro-inflammatory activity are detectable in most tissues[1,59], including the CNS[1,2]. We first confirmed no detectable overexpression of our human TFEB transgene in whole brain lysates of cTFEB;HSACre individuals animals compared to non-transgenic controls (**Figure 3A**).

Hippocampal mRNA levels of pro-inflammatory cytokines previously reported to mediate microglial responses to inflammation in the CNS including *Ccl2* (also known as monocyte chemotactic protein-1, MCP1) [60] and *NFKB*[61] were significantly reduced in the hippocampus of aging female cTFEB;HSACre transgenic mice (**Figure 3B**). Interestingly, levels of *interleukin-6* were significantly elevated in the same groups (**Figure 3B**). Although commonly considered a pro-inflammatory factor, IL-6 also appears to have seemingly contradictory neurotrophic effects in the CNS, increasing neurogenesis[62] and stimulating axon regeneration[63]. Overall, these results suggest a shift in the cytokine transcriptional landscape of the aging hippocampus with upregulated peripheral proteostasis to an overall more anti-inflammatory phenotype, although we did not detect any changes in microglia or astrocyte cell volume or ramification (**Supplemental Figure 3**). Consistent with these findings, we also detected significantly higher levels of expression of Brain Derived Neurotrophic Factor (*BDNF*) in hippocampal lysates from middle-aged (12-month old) female mice (**Figure 3C**), suggestive of an increase in neurotrophic signaling in the aging hippocampus of cTFEB;HSACre transgenic mice.

Accumulation of lipofuscin, a non-degradable intracellular auto-fluorescent polymer, also becomes prominent in the aging brain, likely reflecting an age-associated decline in basal CNS autophagy[1]. We examined the clearance capabilities of the aging CNS by indirect immunofluorescence of lipofuscin granules in brain sections of aged (21 month-old) control and cTFEB:HSACre mice. While we detected striking lipofuscin granule accumulation in several brain regions of aged control mice, including the hippocampus, age- and littermate-matched female cTFEB:HSACre mice revealed a dramatic decrease in lipofuscin deposition, particularly in the dentate gyrus of the hippocampus (**Figure 3D**). Taken together, these results indicate that maintenance of skeletal muscle proteostasis throughout aging reduces

neuroinflammation and promotes maintenance of protein quality control in the aging hippocampus of cTFEB;HSACre transgenic mice.

Improved Performance in Neurocognitive Testing in Aging cTFEB:HSACre Mice.
Geroprotective interventions that target the CNS can have direct effects on brain plasticity, with well-documented benefits on hippocampal-dependent cognitive functions[6,28,39,40]. Given the rejuvenation of proteostasis, reduction in neuroinflammation and increase in *BDNF* expression observed in the aging hippocampi of cTFEB;HSACre transgenic mice, we pursued neurocognitive testing in aged (16-18 months-old) control and cTFEB:HSACre mice (n=10-12/genotype, males and females, littermates). First, we evaluated spatial learning and memory using the Barnes maze task, a hippocampal working memory test known to be sensitive to aging in mice. We documented a significant decrease in the number of errors per trial (**Figure 3E)** and significantly faster escape times (**Figure 3F**) in the Barnes maze test in aged cTFEB:HSACre mice in comparison to controls. Indeed, by the last trial, cTFEB:HSACre mice escaped the maze twice as quickly as control mice. In the novel object recognition task – an independent behavioral test of hippocampal recognition memory – we found that aged cTFEB:HSACre mice exhibited a significantly greater number of contacts with the novel object compared to controls during the test phase (**Figure 3G**). Importantly, we confirmed no difference in visual performance (optomotor test), anxiety (light/dark transfer test), or motor activity (locomotor activity test) between aged control and cTFEB:HSACre cohorts (**Supplementary Figure**). Hence, these results provide exciting evidence for a pronounced improvement in neural function in the aging brain of cTFEB:HSACre mice with enhanced muscle proteostasis.

Neurotrophic Transcriptome Changes in the Hippocampi of cTFEB;HSACre transgenic mice.

To determine the molecular basis of the benefits of enhancing skeletal muscle proteostasis on the aging CNS, we performed unbiased transcriptome analysis on hippocampal RNAs isolated from young (6 months, adult) and aged (21+ months) mice. By this time point, aging animals have demonstrated CNS proteostasis dysfunction (**Figure 3D**), have increased neuroinflammation (**Figure 3B**), and display deficits in cognitive function (**Figure 3E-G**), phenotypes that are significantly improved in cTFEB;HSACre mice.

Bulk RNA-Seq analysis of young hippocampal RNA lysates revealed important changes in gene expression in female (1194 differentially expressed genes, 809 up-regulated and 385 down-regulated) and male (1797 differentially expressed genes, 928 up-regulated and 869 down-regulated) cTFEB;HSACre transgenic mice compared to their age-matched littermate controls (**Figure 4A** and **Supplemental Figure 4**). To identify specific neural signaling functions that could be contributing to the neuroprotective effects of enhancing skeletal muscle proteostasis, we performed GO Enrichment analysis of all differentially expressed genes. In our young groups, we found that key categories associated with synaptic function, including ion- and voltage-gated channel activity, as well as synapse and synaptic membrane categories, were significantly overrepresented in the hippocampus of female cTFEB;HSACre mice (**Figure 4B**). Analysis of the functional enrichment of top differentially expressed genes in the hippocampus of young male cTFEB;HSACre transgenic mice revealed a different pattern, associating instead with multiple mitochondria-targeting pathways (**Supplemental Figure 4**). This included mitochondrial respiratory chain, mitochondrial protein complexes, electron transport chain and ATP metabolic processes (**Supplemental Figure 4**).

Consistent with our biochemical (**Figure 3A-D**) and functional (**Figure 3E-G**) findings suggesting increased neuroprotective benefits in cTFEB;HSACre transgenic mice, we found that these transcriptional changes modulating synaptic function-associated pathways are largely preserved in the aging hippocampus of cTFEB;HSACre transgenic mice (**Figure 4D**). Indeed, functional pathways differentially expressed included learning, memory and in our analysis of the hippocampus of aging cTFEB;HSACre female mice (**Figure 4D**). While overall we detected higher numbers of differentially expressed genes in female aged cTFEB;HSACre transgenic mice (2008 differentially expressed genes) compared to their young cohorts, more than half of those genes were transcriptionally silenced (678 up-regulated and 1330 down-regulated) (**Figure 4C**). We only detected 539 differentially expressed genes in the hippocampus of aged male cTFEB:HSACre transgenic mice (279 up-regulated, 261 down-regulated) (**Supplemental Figure 4**), with only mild significance on GO functional pathways. This is consistent with overall transcriptional dysregulation in the aging CNS, with genes that are dysregulated across multiple brain regions during aging relating to synaptic transmission and plasticity as well as inflammatory or immune-responsive genes[1,3].

Enhanced skeletal muscle proteostasis reduces accumulation of hyperphosphorylated tau and microglial activation in a mouse model of tau pathology.

To assess the potential neuroprotective effects of enhancing skeletal muscle proteostasis in the context of age-associated neurodegenerative disease pathologies, we derived cTFEB;HSACre transgenic mice in the P301S MAPT background. This is a well-known model of neurofibrillary tangle toxicity, a hallmark of AD and related tauopathies[64], and is characterized by prominent hippocampal hyperphosphorylated tau accumulation and neuroinflammation, including microgliosis and astrocyte reactivity[64]. We confirmed muscle-restricted TFEB overexpression in skeletal muscle lysates from P301S MAPT/cTFEB;HSACre mice but no TFEB transgene expression in their P301S MAPT littermates (**Supplemental Figure 5**). We noted that at 9 months of age, when there is robust accumulation of hyperphosphorylated tau and neuroinflammation, and at the onset of behavioral phenotypes in this mouse model[64], we detected a significant reduction in the accumulation of total hyperphosphorylated tau (AT8 phospho-tau antibody) in the dentate gyrus of cTFEB;HSACre;P301S mice compared with single transgenic P301S littermate controls (**Figure 5A**). We also detected similar reductions in levels of 'intracellular tau' in hippocampal cell bodies (**Figure 5A, asterisk**), suggesting reduced accumulation of toxic tau species and aggregates[65] in the hippocampi of cTFEB;HSACre:P301S transgenic mice.

Glial cells, including astrocytes and microglia, are key responders during neuroinflammation, and have been shown to undergo key morphological changes[66] including changes in ramification and cellular process complexity[66], which are believed to reflect reduced immune surveillance activity[67] and increased reactivity phenotypes [68]. Consistent with previous reports in this P301S MAPT tauopathy model[64,69], we confirmed significant increases in the number of GFAP-positive astrocytes (**Figure 5B, middle**), as well as increases in the volume of Iba1-positive microglia in the hippocampus of 9-month-old P301S MAPT mice. Strikingly, we noted significant reductions in these pro-inflammatory associated parameters in the hippocampus of P301S MAPT/cTFEB;HSACre littermates (**Figure 5B, bottom**), suggesting overall reduced neuroinflammation attributed to enhanced skeletal muscle proteostasis during symptomatic disease stages. These biochemical benefits in the CNS of P301S MAPT/cTFEB;HSACre mice were accompanied by re-activation of neurotrophic signaling in the hippocampus, measured by the corrections of declining expression levels of neurotrophic factors BDNF and FNDC5/irisin (**Figure 5C**)[38,70].

Enhancing Skeletal Muscle Proteostasis Reduces Hippocampal Neuroinflammation and Promotes Neurotrophic Signaling in P301S MAPT Transgenic Mice.

To gain more precise insights into neurodegenerative disease relevant transcriptional changes in the hippocampus of cTFEB;HSACre;P301S MAPT mice, we used the Nanostring nCounter® AD panel. This platform directly assesses the expression of 770 genes curated from human and pre-clinical models of AD and robustly captures disease-relevant signatures and their modifications after pre-clinical interventions[71]. Using this approach, we found a total of 79 differentially expressed genes in the cTFEB;HSACre;P301S MAPT+ hippocampi compared to their littermate P301S MAPT+ controls. Interestingly, most differentially regulated genes were downregulated (76 of 79), consistent with their identity as transcriptional drivers of disease[71]. Many of these transcripts are associated with microglial activation (including *Rhoc*, *Alcam*, *Scamp2*, *Syngr11* and *Csf1*) and apoptosis (*PI3kR1*), consistent with increased neuroprotection and reduced neuroinflammation in the hippocampus of P301S MAPT/cTFEB;HSACre mice with enhanced skeletal muscle proteostasis (**Figure 5D**). Indeed, functional annotation of the co-expression/functional clusters revealed significant reductions in microglial activation modules (**Figure 5E**) in the hippocampi of 9 month old female cTFEB;HSACre:P301S mice compared with P301S littermates **(Figure 5E**). Interestingly, one of the most significantly downregulated transcripts was *Arhgdib,* which was recently identified as a potential novel biomarker for neurofibrillary tangle accumulation and neuropathological Braak stage in human entorhinal cortex[72], suggesting a novel potential neurotrophic mechanism that can slow down accumulation of tau tangles in the CNS. Consistent with this hypothesis, we also detected significant reductions in disease-associated expression of proteostasis-associated genes (*Hsp90aa1,* coding for heat shock protein-90 and *Hsbp1,* coding for small heat-shock protein 27). In this current study, we only observed 3 significantly up-regulated transcripts, *Rsg7*, *Dop1A* and *Tgm2*. Little is known about these genes in the context of AD, but all three are part of the nCounter Panel due to strong and consistent dysregulation in AD-states in both animal models and human studies[71,73]. Similar analysis of male hippocampal RNA revealed only 32 differentially expressed genes (19 down regulated genes, 13 up regulated genes) between cTFEB;HSACre:P301S MAPT and P301S MAPT transgenic mice, with similar down-regulation of pathway members of the microglia activation cluster (*Bcar3, Scna*), axon and dendrite structure (*Prex1*) and transmitter release (*Atp2b2, Ywhag, Synj1*). These provocative results suggest that enhanced skeletal muscle proteostasis modifies the accumulation of pathogenic tau isoforms and reduces neuroinflammation in the hippocampus of P301S mice via activation of neurotrophic signaling in the CNS.

DISCUSSION

Skeletal muscle comprises roughly 40% of the total body mass in a healthy young adult human and is highly susceptible to age-associated proteostatic decline[55,74]. Muscle autophagy facilitates metabolic reprogramming and mitochondrial quality control during conditions of high metabolic demand[16,75,76], and is also required to maintain muscle health and muscle mass[77,78 79]. Skeletal muscle health has been linked to multiple chronic age-associated conditions, including diabetes[80], cardiovascular disease[81] and, more recently, neurodegenerative diseases[36,37,39]. In agreement with this, muscle-originating circulating factors (myokines) appear to play central roles in regulating CNS health and function. For example, Amyrel amylase, a skeletal muscle secreted protein with maltose producing function, was recently identified as a key proteostasis stress-induced myokine with CNS targeting effects in *Drosophila Melanogaster*[18]. GFP-tagged Amyrel overexpressed in skeletal muscle is detected in the fly circulation, and muscle-specific *amyrel* overexpression improves proteostasis and prevents neurodegeneration induced by aggregation-prone disease-associated pathogenic proteins in the fly brain and retina[18]. Fibronectin-domain III containing 5 (FNDC5) is a glycosylated type 1 membrane protein that is highly enriched in skeletal muscle and can be proteolytically cleaved into an N-terminal fragment known as irisin, which is then released into circulation[80]. Recent studies have demonstrated that peripheral delivery of irisin reduces neuroinflammation and rescues cognitive decline in two separate mouse models of AD[32]. Likewise, the lysosomal protease Cathepsin B is secreted from skeletal muscle into circulation in response to exercise and is required for the full manifestation of exercise-associated benefits on the CNS, including increases in the levels of hippocampal BDNF and re-activation of neurogenesis[33]. This suggests that maintenance of the skeletal muscle 'secretome' may be central to the regulation of CNS aging and disease.

Here, and for the first time, we provide direct evidence for the CNS benefits of maintaining skeletal muscle proteostasis throughout aging. We find that mild overexpression of TFEB in skeletal muscle in cTFEB;HSACre transgenic mice reduces the development of age-associated phenotypes in the hippocampus. Importantly, we document that these benefits occur without any detectable expression of our transgene in the CNS, suggesting that the observed reductions in proteotoxicity and improvements in neurocognitive function are due to the overexpression of TFEB solely in the skeletal muscle. To date, multiple studies have repeatedly reported that genes that are downregulated across multiple brain regions during aging are enriched with genes related to synaptic transmission and plasticity (reviewed here[3]). Furthermore, in-depth transcriptional studies of the aging mouse brain point to key metabolic

pathways, the dysregulation of ion homeostasis, disruption of neurotransmission and ribosome biogenesis as key biological process exhibiting differential regulation with aging[2,82]. It is particularly interesting that manipulation of skeletal muscle proteostasis modulates expression of similar key functional enrichment categories in the aging hippocampus (**Figure 4**), suggesting an important transcriptional remodeling of the aging CNS with memory and cognition benefits in response to skeletal muscle TFEB-expression.

In addition to demonstrating the benefits of maintaining skeletal muscle proteostasis on the aging CNS, our findings also suggest important benefits associated with enhancing skeletal muscle proteostasis in the context of tau-pathology. Tauopathies are clinically, biochemically and morphologically heterogenous neurodegenerative diseases characterized by the deposition of abnormal aggregates of tau in the brain. The MAPT P301S model recapitulates multiple aspects of tauopathies, including microglial activation, synapse loss and filamentous tau inclusions[64]. Our studies indicate that enhancing skeletal muscle proteostasis has significant benefits on multiple markers of gliosis, including reduced number of astrocytes and reduced microglial volume in the hippocampus of female cTFEB;HSACre;MAPT P301S, as well as a significantly reduced transcriptional activation of the nCounter AD microglial activation panel. This suggests that one potential mechanism underlying the benefits of enhancing muscle proteostasis in MAPT P301S transgenic mice is through reducing microglial and astrocyte activation, ultimately reducing neuroinflammation. Interestingly, two of the differentially expressed genes in our nCounter AD panel run are cellular chaperones have been reported to directly coordinate tau protein homeostasis[83,84]. Given the reduced levels of tau accumulation in cTFEB;HSACre;P301S MAPT+ hippocampi, one possibility is that by this time point, the compensatory expression of these chaperones in response to the accumulation of the aggregation prone P301S MAPT protein is no longer required, although this hypothesis remains untested.

Through our proteomics analysis, we identified multiple differentially expressed proteins in TFEB-overexpressing skeletal muscle that are predicted to be secreted through classical and non-classical mechanisms. Surprisingly, our highest expressed factor was cathepsin B, a myokine with known CNS targeting benefits[33]. Circulating factors with neurotrophic effects have direct receptors at the blood-brain barrier interface or can, to some degree, cross it[25,29,32,33]. We have determined elevation of several of these factors (cathepsin B, irisin, IGF-1, BDNF) in the periphery of cTFEB;HSACre transgenic mice, suggesting potential mechanisms for our reported CNS benefits. Interestingly, several of these factors have been reported to work through

inhibition of neuroinflammation[23,27,28,32], consistent with our findings in the hippocampus of aging and MAPT P301S mice with enhanced skeletal muscle proteostasis. Although the mechanisms responsible for the transduction of these neurotrophic, anti-inflammatory signals into the hippocampus remain poorly understood, some evidence suggests that astrocytes at the blood-brain barrier interface monitor cerebral perfusion and control systemic circulation to maintain brain blood flow[85]. This suggests that astrocytes may act as central sensors of peripheral signals in circulation. In agreement with this, we observed significant changes in astrocyte numbers and microglial process complexity in the hippocampus of cTFEB;HSACre;MAPT P301S transgenic mice, suggesting a concerted glial response in response to enhanced skeletal muscle proteostasis.

Over the last ten years, there has been growing evidence that suggests prominent contributions of the periphery to the etiology of neurodegenerative diseases. Our discovery that skeletal muscle proteostasis can be a crucial site for CNS health and function regulation provides compelling evidence for a new therapeutic delivery avenue into the brain, providing novel and current unexplored potential diagnostic and therapeutic intervention sites, and potentially accelerating future clinical trial design and implementation.

METHODS

Generation of fxSTOP-TFEB transgenic mice.

We used a pCMV-human TFEB expressing vector from Origene (clone # sc122773), previously used here [40]. We cloned a 3X-Flag fragment via insertion into the Acc65I and Pac1 restriction sites of the targeting vector. The fxSTOP-TFEB vector was generated in multiple steps, as follows: (1) 5′ and 3′ targeting arms were inserted by PCR onto the ends of a minimal 1.8 kb, chloramphenicol-resistant vector; (2) an ampicillin resistance cassette was cloned into the MluI, XmaI sites of the targeting vector; (3) an 1.1 kb fragment encoding the actin promoter, a loxP site, a 3XFLAG tag fused to EGFP was cloned into the NheI, PacI restriction sites of the targeting vector; (4) a 2.8 kb fragment containing the second loxP site, followed by 3XFLAG-human TFEB sequence. The final fxSTOP-Flag-human TFEB vector was microinjected into C57BL/6J:C3H/HeJ F1 hybrid oocytes. Of six founders identified, two gave rise to fxSTOP-Flag-human TFEB lines with comparable phenotypes. Of these lines, we chose to focus our studies principally on line 419. The presence of the floxed 3x-FLAG-eGFP STOP-3x-FLAG-human TFEB cassette is verified by allele dependent qPCR genotyping analysis with each generation

(Transnetyx), and expression of the 3x-FLAG-eGFP sequence (upstream of the STOP codon) in single transgenic fxSTOP-TFEB mice is assessed every other generation. We confirmed excision of 3XFLAG-EGFP-STOP cassette in the presence of Cre-recombinase by crossing fxSTOP-TFEB transgenic female mice with HSA-Cre transgenic mice, obtained from JAX (Stock No: 006139 | HSA-Cre79), and corresponds to the HSA-Cre driver mouse line from the laboratory of Dr. Judith Melki. The P301S MAPT line was also obtained from JAX (Stock No: 008169) and originated in the laboratory of Dr. Virginia Lee. cTFEB;HSACre;MAPT P301S transgenic mice were generated by crossing fxSTOP-TFEB females to MAPT P301S males. Female double transgenic offspring was then crossed with homozygote HSA-Cre transgenic males. All lines are maintained in a C57/B6 background for over ten generations in our lab. Age-matched littermates were used for all experiments. Mice were housed in a temperature- and humidity-controlled environment on a 12-hour light/dark cycle with food and water ad libitum. Mice of both sexes were used for all experiments in equal numbers, or as close to equal numbers as possible. All animal experimentation adhered to NIH guidelines and was approved by and performed in accordance with the University of California, San Diego, Duke University and University of Alabama at Birmingham Institutional Animal Care and Use.

Tissue Collections

Animals were anesthetized with 3.8% Avertin Solution. All animals received a transcardial perfusion with 60 mLs of cold 1x PBS. Half of the tissue (right/left muscle, right/left hemi-brain) was post-fixed in 4% PFA for less than 24 hours before being transferred to 30% sucrose for another 24 hrs, the other half was flash-frozen in liquid nitrogen for RNA and protein analyses.

RT-PCR Analysis

Flash frozen perfused isolated mouse tissues (Quadricep, Hippocampus) were placed in plastic tubes with silica beads (MP Biomedical #116913100) and homogenized in TRIzol (Invitrogen # 15596026). RNA was extracted via standard phenol-chloroform procedures followed by DNase digestion (Thermo Fisher #AM2238). cDNA was generated using iScript (Bio-Rad Technologies #1708891). Quantitative PCR was run using Sybrgreen (Life Technologies # 4309155) for chemical detection (Applied Biosystems; QuantStudio 3). Enrichment was determined based on double-delta CT value. Primers were ordered from IDT Predesigned qPCR Assays unless otherwise specified. Primers used were Actin-beta mm.pt.39a.22214843.g.

ImmunoBlot Analysis

Protein lysates from muscle tissue was prepared as previously described (Cortes et al 2014, Sopher et al 2004). Protein concentration was quantified using a Pierce™ BCA Protein Assay (#23227). Fifty µg of homogenized proteins per lane, and after running Any KD, 10%, or 4-15% Mini-PROTEAN TGX Gels (4568124, 4561034, 4561084, BioRad), samples were transferred to 0.2 or 0.45 µm PVDF membranes (162-0175, 1704275, BioRad), which were blocked in 5% BSA in PBS at RT for 1 hr. Membranes were incubated with anti-Lamp1 antibody (NB600-956, Novus Bio), anti-LC3 antibody (2775S, Cell Signaling), anti-p62(PM045, MBC), or anti-GAPDH (AM4300, Invitrogen) in PBS-T with 5% BSA at 4°C overnight. The primary antibody was visualized with horseradish-peroxidase conjugated anti-rabbit at 1:5,000 (7074P2, Cell Signaling) and enhanced chemiluminescence (170-5060, BioRad) or goat-anti-mouse IgG 680 (A21058,Invitrogen) at 1:10,000. Densitometry analysis was performed using the BioRad Image Lab 6.1 software application. Unpaired t-tests were used in Graphpad Prism on GAPDH and control- normalized data.

Cytokine Array

120 µL of serum, or 50 µg of protein lysates from muscle and brain tissue, were loaded on to membranes of the cytokine array kit (Abcam ab193659). Membranes were incubated in blocking buffer solution at room temperature for 30 minutes, and washed 3 times with wash buffer for 5 minutes each. Membranes were incubated with 1 mL of 1X biotinylated antibody cocktail overnight at 4°C, then incubated with 2 mL of 1X HRP-Conjugated Streptavidin for 2 hours at RT. Each membrane was then transferred face up onto a sheet of chromatography paper and received 250 µL of Detection Buffer C and Detection Buffer D respectively (500 µL total).

Histological Studies

Tissue was embedded in OCT (TissueTek/4583), frozen utilizing 2-methylbutane (VWR, 103525-278) submerged in liquid nitrogen and stored at -80C until used. All samples were sectioned on a standing cryostat (Leica). Sections of brain were 20 microns, while muscle tissue was 15 microns thick. For immunohistochemistry, sections were permeabilized with .25% Triton for 15 mins and blocked with 4% BSA for 30 minutes-1 hour. Sections were then incubated with primary antibodies overnight at 4°C and incubated with secondary antibodies at RT for 1 hour (both diluted in 4% BSA). Next the slides were washed with Hoescht (Thermo Scientific 62249) and mounted with prolong glass (Invitrogen P36984). All slides were washed with 1X PBS three times for 5 minutes each between steps.

Slides were imaged in the UAB HIRF HRIF Confocal/Light Microscopy Core utilizing the 10x objective on the Nikon A15R/SIM Confocal microscope. Z-stacks were collected, and max intensity projections were generated using FIJI. The lipofuscin imaging was done using an epifluorescent Nikon light microscope using the 20x objective.

For quantification of astrocyte and/or microglia parameters, raw ND2 files were uploaded to the NIS elements platform and thresholds were set to eliminate background in each channel in order to delineate each object. Morphometric information was collected in addition to the automated counting of objects. A size exclusion parameter was used and GFAP positive objects under 10 microns, Iba-1 positive objects under 15 microns, and any object larger than 5,000 microns were all excluded due to standard assessments of cell sizes.

Quantitative proteomics sample preparation and data-independent acquisition mass spectrometry.

We identified distinct protein species from crude total extractions of whole quadriceps muscle by mass spectrometry after trypsin digestion, in collaboration with the University of Washington Nathan Shock Center Protein Phenotypes of Aging Proteomics Core. Quadriceps muscle powder samples were processed and digested using S-Trap Micro Spin Column (Protifi, C02-micro-80) following the manufacturer's protocol. SDS (5%) lysis and solubilization buffer were added to liver powder samples and homogenized on ice using a sonicator probe. Protein concentrations were determined using Pierce BCA Protein Assay Kit (Thermo Fisher Scientific, PI23227). Proteins were digested at 1 ug trypsin to 25 ug protein ratio on S-Trap at 47°C for 1 h. Peptides extracted from S-Trap were dried with a vacuum concentrator and reconstituted in 0.1% formic acid in water prior to mass spectrometry acquisition. Data were acquired using data-independent acquisition (DIA) on a Thermo EASY-nLC 1000 and a Thermo Q-Exactive HF orbitrap mass spectrometer. Peptides were separated using PicoFrit Self-Packed Columns (360 µm OD x 75 µm ID; New Objective, Woburn, MA) packed to 30 cm with 3 µm ReproSil-Pur C18 beads (ESI Source Solutions, r13.aq.0001). The trap column was packed to 2 cm with same C18 beads using 360 µm OD x 150 µm ID fused silica capillary fritted with Kasil on one end. Solvent A was 0.1% formic acid in water, and solvent B was 0.1% formic acid in 80% acetonitrile. For each injection, 1 µg of sample was loaded and eluted using a 90-min gradient from 5% to 45% B at 250 nL/min. DIA methods followed the chromatogram library workflow as described in detail previously [86]. All muscle samples were pooled in equal ratio to create a muscle library sample. The library samples were used to generate chromatogram libraries using the strategy described before [87]. Thermo Q Exactive HF MS was used to acquire six gas phase

fractionated runs spanning a total mass range of 400 to 1000 m/z, each with staggered 4 m/z narrow precursor isolation windows [88]. EncyclopeDIA software suite was used to generate a chromatogram library [86] and retention time models for all peptides detected at 1% FDR determined by Percolator [89]. For quantitative DIA run, equal amounts of protein were used for each sample. A 24 × 24 m/z staggered window from 400.43190 to 1000.7048 m/z was used as described previously [88]. EncyclopeDIA software suite was used to search the chromatogram library with calibrated retention time and quantify peptides and proteins in each sample.

Proteomics Analysis

A linear model was fit to the protein level data using the Bioconductor limma package [90], and the estimated SVs were adjusted as covariates in our model. The limma package uses empirical Bayes moderated statistics, which improves power by 'borrowing strength' between proteins in order to moderate the residual variance [91]. Adjusted P value was calculated with Benjamini-Hochberg method across groups (young transgenic, young control, old transgenic, and old control). An FDR cutoff of 10% was selected. Protein hits were entered into an Excel spreadsheet: "Connie_Cortes_SKM_proteomics_pid1910_IPA.xlsx", where proteins are in rows and each column shows the logFC (log 2 fold-change), P.value (raw P.value) and adjusted P.Value.

Proteins were sorted for significant differential expression with dplyr using a cutoff of less than 5% FDR and greater than $|\pm 0.58496|$ $\log_2$ foldchange in young and old cohorts as a change due to skeletal muscle overexpression of humanized TFEB. Volcano plots were created with ggplot and ggrepel. Significantly upregulated proteins in cTFEB;HSA-Cre mice were queried using the KEGG pathway analyzer, which is a feature of STRING's web tool [57]. Bar graphs were created in Rstudio with the ggplot2 and forcats packages.

Significantly upregulated proteins, up to two degrees from TFEB, were entered into STRINGdb for functional network analysis. A confidence interaction score of 0.70 and MCL clustering was applied to the networks. The networks were exported from STRING and imported into Cytoscape for further style editing [92]. Predicted secreted proteins were identified by comparing the significantly differentially expressed proteins to the mus musculus secretome from VerSeDa[58].

Gene Expression Analysis.

RNA Sequencing

RNA was extract as mentioned above from flash frozen hippocampal tissue or tissue was extracted by Novogene (Novogene Corporation INC, Sacramento, CA, United States) for four biological replicates (sex/genotype) and checked for quality. mRNA libraries were prepared by Novogene and bulk RNA-seq analysis was performed via NovaSeq PE150 (Illumina, San Diego, CA, United States) high throughput sequencing.

Nanostring

Assays were performed with 100 ng aliquots of RNA using the NanoString nCounter Analysis system (NanoString Technologies, Seattle, WA, USA) on 9 month-old male and female MAPT P301S and cTFEB;HSACre;MAPT P301S hippocampus, following previously described and established protocols [71]. Counts for target genes were normalized to house-keeping genes (*Cltc, Gapdh, Gusb, Hprt, Pgk1, Tubb5*). After codeset hybridization overnight, the samples were washed and immobilized to a cartridge using the NanoString nCounter Prep Station. Cartridges were scanned in the nCounter Digital Analyzer at 555 fields of view for the maximum level of sensitivity. Gene expression was normalized using NanoStringNorm R package. Specifically, background correction was performed using the negative control at the cutoff of mean + 2 standard deviation. All p values were adjusted using a false discovery rate (FDR) correction of 1% for multiple comparisons. Housekeeping genes were used to for normalization based on geometric mean. Data and heat analyses were performed in the nSolver Analysis Software 2.0. Nanostring experiments were conducted at the UAB Nanostring Core. Gene expression values were presented as the percentage of the MAPT P301S group for comparison of MAPT P301S pathogenesis to the cTFEB;HSACre;MAPT P301S cohort.

Mouse Phenotyping and Behavioral Studies.

Barnes Maze

The Barnes maze apparatus is an opaque Plexiglas disc 75 cm in diameter elevated 58 cm above the floor by a tripod. Twenty holes, 5 cm in diameter, are located 5 cm from the perimeter, and a black Plexiglas escape box (19 x 8 x 7 cm) is placed under one of the holes. Distinct spatial cues are located all around the maze and are kept constant throughout the study. On the first day of testing, a training session was performed, which consists of placing the mouse in the escape box for one minute. After the one minute habituation period, the first

session was started. At the beginning of each session, the mouse was placed in the middle of the maze in a 10 cm high cylindrical black start chamber. After 10 seconds the start chamber was removed, a buzzer (80 dB) and a light (400 lux) were turned on, and the mouse was set free to explore the maze. The session ended when the mouse entered the escape tunnel or after 3 min elapsed. When the mouse entered the escape tunnel, the buzzer was turned off and the mouse was allowed to remain in the dark for one minute. When the mouse did not enter the tunnel by itself it was gently put in the escape box for one minute. The tunnel was always located underneath the same hole (stable within the spatial environment), which was randomly determined for each mouse. Mice were tested once a day for 4 days for the acquisition portion of the study. For the 5th test (probe test), the escape tunnel was removed and the mouse was allowed to freely explore the maze for 3 min. The time spent in each quadrant was determined and the percent time spent in the target quadrant (the one originally containing the escape box) was compared with the average percent time in the other three quadrants. This was a direct test of spatial memory as there was no potential for local cues to be used in the mouse's behavioral decision. Two weeks later the mice were tested again with the escape box in the original position (retention test). This allows for the examination of long term memory. Finally, on the day after this test, the escape tunnel was moved to a new location (90 degrees from the original position) and the behavior of the mouse was recorded. This is called the reversal test and it allows for the examination of perseveration at the old hole as well as the working memory strategies the mice adopted to locate the new tunnel location. Each session was videotaped and scored by an experimenter blind to the genotype of the mouse. Measures recorded include the latency to enter the escape box and the number of errors made per session. Errors are defined as nose pokes and head deflections over any hole that did not have the tunnel beneath it. The probe data were analyzed using Noldus Ethovision software to determine time spent in each quadrant of the maze as well as to assess activity measures.

Novel Object Recognition

Mice were individually habituated to a 51cm x 51cm x 39cm open field for 5 min. Mice were then tested with two identical objects placed in the field (either two 250 ml amber bottles or two clear plastic cylinders 6x6x16cm half filled with glass marbles). An individual animal was allowed to explore for 5 min, now with the objects present. After two such trials (each separated by 1 minute in a holding cage), the mouse was tested in the object novelty recognition test in which a novel object replaced one of the familiar objects (for example, an amber bottle if the cylinders were initially used). All objects and the arena were thoroughly cleaned with 70% ethanol

between trials to remove odors. Behavior was video recorded and then scored for number contacts (touching with nose or nose pointing at object and within 0.5 cm of object) and/or for time contacting the objects. Habituation to the objects across the familiarization trials (decreased contacts) was an initial measure of learning and then renewed interest (increased contacts) in the new object indicated successful object memory. Recognition indexes were calculated using the following formula: # contacts during test/(# contacts in last familiarization trial + # contacts during test). Values greater than 0.5 indicate increased interest, whereas values less than 0.5 indicate decreased interest in the object during the test relative to the final familiarization trial.

Neurological Disease Scoring

For neurological dysfunction studies (P301S MAPT mice), mice were visually inspected by a blinded examiner for obvious neurological signs and examined using a composite neurological evaluation tool (ledge test, clasping, kyphosis and gait were scored on a scale of 0 (normal) to 3 (severely impaired)), as described previously [93]. Females and males were used in equal numbers, or as close to equal numbers as possible, and studies were performed by a blinded examiner. For survival studies, animals were monitored daily and pronounced dead when respiration or heartbeat was no longer present, and/or humanely euthanized upon limb paralysis and inability to access food/water.

Statistical Analysis

All data were analyzed by t-test, chi-square, or 2-way between-subject ANOVA with Tukey post hoc comparisons depending on the number of variables and groups in each analysis. HRR and ROS production were analyzed by 2-way (genotype × complex activity) between-subject ANOVA. Survival curves were analyzed using Log-rank (Mantel-Cox) Test. Data were analyzed using Prism 7 (GraphPad Software, La Jolla, CA) and are represented as means and standard error of the means. All experiments and data analyses were conducted in a blinded fashion.

All data were prepared for analysis with standard spread sheet software (Microsoft Excel). Statistical analysis was done using Microsoft Excel or Prism 4.0 (Graph Pad). For ANOVA, if statistical significance ($p < 0.05$) was achieved, we performed post hoc analysis to account for multiple comparisons. The level of significance (α) was always set at 0.05.

FIGURE LEGENDS

Figure 1: Generation and validation of muscle-specific TFEB overexpressing mice. (a) Schematic depicting 3x-FLAG-human TFEB transgene. Cassettes are arranged from 5' (left) to 3' (right), with the β-actin promoter with CMV enhancer on the far 5' end, and a 3x-FLAG-eGFP STOP cassette flanked by loxP sites just 5' from the 3x-FLAG-human TFEB transgene. (b) Immunoblot of control (left) and cTFEB;HSACre (right) skeletal muscle lysates. Humanized TFEB weighs ~64 kDa (purple arrow), while endogenous mouse TFEB weighs ~51 kDa (gold arrow). Quantification of total TFEB protein levels (right), AU values are normalized to tubulin and control TFEB expression. (c) Immunohistochemistry of Flag stain (green) and DAPI (blue) in skeletal muscle tissue. (d) RT-PCR of skeletal muscle lysates depicts significantly higher expression of Atg5, Cathepsin D, and Lamp1 in cTFEB;HSACre mice. (e) Immunoblot analysis of skeletal muscle lysates depicts significantly higher levels of LAMP-1, Cathepsin D, and LC3II protein. Data are represented as mean± SEM * $p<0.05$, ** $p<0.01$, T-test, Scale bars: 20 μm

Figure 2: Proteomics Analysis Identifies Increased Proteostasis Related Proteins in TFEB-Overexpressing Skeletal Muscle. (a-b) Volcano plot depicting differentially regulated proteins in 6-month-old (a) and 18-month old(b) cTFEB;HSACre mice relative to control. Note that TFEB protein itself is highly expressed in both old and young (purple rectangles). (c) KEGG enrichment analysis grouping differentially regulated proteins into categories associated with proteostasis and autophagy (pink), Mitochondrial metabolism (gold), fatty acid metabolism (green), age-associated signaling (blue), and amino acid metabolism (purple). (d) STRING protein-protein interactions depicted differentially regulated proteins predicted to interact with TFEB (blue) and Mtor (green). (e) VerSeDa predicted secreted proteins differentially expressed in young (blue) and aged (green) cTFEB;HSACre mice. (f) Immunoblot analysis of cathepsin B protein. Note that the smaller, mature fragment of Cathepsin B is the secreted form. (g) Elevated levels of cathepsin B in serum from cTFEB;HSACre mice. Data are represented as mean± SEM * $p<0.05$, ** $p<0.01$, T-test.

Figure 3: Peripheral Over-expression of TFEB decreases neuroinflammation, lipofuscin accumulation, and rescues behavior in aged mice. (a) Hemibrains of control (left) and cTFEB;HSACre (right) mice were flash frozen and protein was extracted. Staining for anti-TFFB antibody shows endogenous levels of protein expression were consistent between controls and bigenic animals. Notably, there is a lack of humanized TFEB expression in the CNS of cTFEB;HSACre mice (compare to Figure 1B). (b) RT-PCR of hippocampal lysates from 18 month old female mice. Decreased expression or CCL2 and NFKB, and increased expression of IL6 was detected in cTFEB;HSACre mice, n=11. (c) RT-PCR of 12 month old female hippocampal lysates. Increased relative expression of BDNF in hippocampi of cTFEB;HSACre mice relative to age-matched control littermates. N=12 animals. (d) Hemibrains of 18 month+ control and cTFEB;HSACre mice were stained for DAPI and imaged. The dentate of the hippocampus was focused on and imaged (Hoescht-Blue), and one channel was left open in order to capture autofluoresecence (green). The auto-fluorescent punctae were identified as lipofuscin particles. We observed a non-significant decrease in the number of Lipofuscin punctae in the CNS of cTFEB;HSACre mice compared to their control littermates. Data are represented as mean± SEM * $p<0.05$, ** $p<0.01$, T-test (e-g) Neurocognitive battery of 18 month old female cTFEB;HSACre and control animals. cTFEB;HSACre mice made significantly less errors (e) and escaped the barnes maze more quickly (f) than their wild type controls. Additionally, cTFEB;HSACre mice made significantly more contacts with the novel object than their age-matched control littermates (g). Data are represented as mean ± SEM * $p<0.05$, ** $p<0.01$, One-way ANOVA, post-hoc T-test, Scale bar: 20 μm. Scale bars = 100 μm.

Figure 4: Neurotrophic Transcriptome Changes in the Hippocampi of cTFEB;HSACre transgenic mice. (a) Transcriptomics of differentially expressed genes in the hippocampi of young female cTFEB;HSACre mice. (b) GO term analysis of differentially expressed genes in the hippocampi of young female cTFEB;HSACre mice. (c) Transcription changes associated with increased peripheral TFEB expression in old female cTFEB;HSACre mice. (d) GO term analysis of differentially expressed genes in the hippocampi of old cTFEB;HSACre mice.

Figure 5: Enhanced skeletal muscle proteostasis reduces accumulation of hyperphosphorylated tau and microglial activation in a mouse model of tau pathology. (a) Immunohistochemistry depicting PhosphoTau staining (gray) and Hoescht staining (blue) in the hippocampal dentate gyrus of Control (top) P301S MAPT (middle), and triple transgenic P301S MAPT/cTFEB;HSACre mice (bottom). Insets depicting intracellular PTau are 5X zooms of areas demarcated by yellow squares. Scale bars = 100 μm. Quantification of total Phosphotau tangles/section for both sexes of the three genotypes (right) and for intracellular Phosphotau tangles (Phosphotau staining overlapping with at least one pixel of Hoescht). (b) Immunohistochemistry of GFAP (green), Iba1 (red), and Hoescht (blue) staining in the dentate gyrus of Control (top) P301S MAPT (middle), and triple transgenic P301S MAPT/cTFEB;HSACre mice (bottom). Insets depicting glia morphology are 5X zooms of areas demarcated by yellow squares. Scale bars = 100 μm. Quantification for GFAP object number per section and process complexity (top right) and Iba1+ object volume and process complexity (bottom right) for male and female mice of the three genotypes. (c-d) RT-PCR of 9 month old female hippocampal lysates from the three aforementioned genotypes. Increased relative expression of BDNF (c) and FNDC5 (d) comparable to Control levels in hippocampi of P301S MAPT/cTFEB;HSACre mice relative to age-matched P301S MAPT littermates. Data are represented as mean± SEM * $p<0.05$, ** $p<0.01$, One-way ANOVA, post-hoc T-test. (e) Transcriptional expression of differentially regulated genes in the hippocampi of P301S MAPT/cTFEB:HSACre animals relative to age-matched P301S MAPT littermates. (f) Genes associated microglial activation downregulated in P301S MAPT/cTFEB;HSACre compared to P301S MAPT age-matched littermates. Analysis done via nSolver (Nanostring) differential gene expression analysis software.

Supplemental Legends

Supplemental Figure 1
(a)RT-PCR of myostatin expression in quadriceps muscle of aged female cTFEB;HSACre and age matched control littermates. (b) RT-PCR of Atg5, Cathepsin D, and Lamp1 in young female quadcriceps.

Supplemental Figure 2
(a)STRING predicted protein-protein interactions in quadriceps of cTFEB;HSACre male mice. (b) RT-PCR of Cathepsin B in quadriceps of cTFEB;HSACre male (triangles) and female (circles) mice compared to age-matched control littermates.

Supplemental Figure 3
(a)IHC of 18 month+ animals was stained for Iba1 (red) and Hoescht (blue) in control (top) and cTFEB;HSACre (bottom) mice. Quantification of Iba1+ object volume (top right) and Iba1+ object surface/volume ratio (bottom right). Scale bars = 100 µm. (b) Staining for GFAP (green) and hoescht (blue) in the hippocampi of control (top) and cTFEB;HSACre (bottom) mice. Quantification of average number of GFAP+ objects per section (top) and GFAP+ object surface to volume ratio (bottom) for male (triangles) and female (circles) mice. (c) Quantification of average number of lipofuscin punctae in the hippocampi of aged male cTFEB;HSACre and age matched control littermates.(d) Barnes maze number of errors/trail and latency to escape in male mice.

Supplemental Figure 4
(a) Transcriptomics analysis depicting differentially expressed genes in young male cTFEB;HSACre hippocampi relative to age-matched control littermates. (b) GO term analysis of differentially expressed genes in the hippocampi of young male cTFEB;HSACre mice. (c) Transcriptomics analysis depicting differentially expressed genes in old male cTFEB;HSACre hippocampi relative to age-matched control littermates. (d) GO term analysis of differentially expressed genes in the hippocampi of old male cTFEB;HSACre mice.(e) GO term analysis of young (left) and old (right) female mice. (f) GO term analysis of young (left) and old (right) male mice.

Supplemental Figure 5
(a)Immunoblot analysis of quadriceps lysates from P301S MAPT (left bands) and P301S MAPT/cTFEB;HSACre (right bands) mice staining for 3xFlag TFEB. GAPDH band on bottom. (b) Transcriptional changes in the hippocampi of male P301S MAPT/cTFEB;HSACre mice relative to age-matched P301S MAPT littermates. Shift in genes associated with Apoptosis (c), Lipid metabolism (d). and Trophic factors (e) in hippocampi from P301S MAPT mice (left) and P301S MAPT/cTFEB;HSACre (right) mice. Additionally, the nanostring panel groups genes associated with AD into 3 color categories (f-h).

REFERENCES

1 Lopez-Otin, C., Blasco, M. A., Partridge, L., Serrano, M. & Kroemer, G. The hallmarks of aging. *Cell* **153**, 1194-1217, doi:10.1016/j.cell.2013.05.039 (2013).

2 Mattson, M. P. & Arumugam, T. V. Hallmarks of Brain Aging: Adaptive and Pathological Modification by Metabolic States. *Cell Metab* **27**, 1176-1199, doi:10.1016/j.cmet.2018.05.011 (2018).

3 Ham, S. & Lee, S. V. Advances in transcriptome analysis of human brain aging. *Exp Mol Med* **52**, 1787-1797, doi:10.1038/s12276-020-00522-6 (2020).

4 Aman, Y. *et al.* Autophagy in healthy aging and disease. *Nat Aging* **1**, 634-650, doi:10.1038/s43587-021-00098-4 (2021).

5 Hara, T. *et al.* Suppression of basal autophagy in neural cells causes neurodegenerative disease in mice. *Nature* **441**, 885-889, doi:10.1038/nature04724 (2006).

6 Komatsu, M. *et al.* Loss of autophagy in the central nervous system causes neurodegeneration in mice. *Nature* **441**, 880-884, doi:10.1038/nature04723 (2006).

7 Mansueto, G. *et al.* Transcription Factor EB Controls Metabolic Flexibility during Exercise. *Cell Metab* **25**, 182-196, doi:10.1016/j.cmet.2016.11.003 (2017).

8 Kim, K. H. *et al.* Autophagy deficiency leads to protection from obesity and insulin resistance by inducing Fgf21 as a mitokine. *Nat Med* **19**, 83-92, doi:10.1038/nm.3014 (2013).

9 Kustermann, M. *et al.* Loss of the novel Vcp (valosin containing protein) interactor Washc4 interferes with autophagy-mediated proteostasis in striated muscle and leads to myopathy in vivo. *Autophagy* **14**, 1911-1927, doi:10.1080/15548627.2018.1491491 (2018).

10 Lapierre, L. R. *et al.* The TFEB orthologue HLH-30 regulates autophagy and modulates longevity in Caenorhabditis elegans. *Nat Commun* **4**, 2267, doi:10.1038/ncomms3267 (2013).

11 Pyo, J. O. *et al.* Overexpression of Atg5 in mice activates autophagy and extends lifespan. *Nat Commun* **4**, 2300, doi:10.1038/ncomms3300 (2013).

12 Simonsen, A. *et al.* Promoting basal levels of autophagy in the nervous system enhances longevity and oxidant resistance in adult Drosophila. *Autophagy* **4**, 176-184, doi:5269 [pii] (2008).

13 Colman, R. J. *et al.* Caloric restriction delays disease onset and mortality in rhesus monkeys. *Science* **325**, 201-204, doi:10.1126/science.1173635 (2009).

14 Eisenberg, T. *et al.* Induction of autophagy by spermidine promotes longevity. *Nat Cell Biol* **11**, 1305-1314, doi:10.1038/ncb1975 (2009).

15 Harrison, D. E. *et al.* Rapamycin fed late in life extends lifespan in genetically heterogeneous mice. *Nature* **460**, 392-395, doi:10.1038/nature08221 (2009).

16 Settembre, C. *et al.* TFEB controls cellular lipid metabolism through a starvation-induced autoregulatory loop. *Nature cell biology* **15**, 647-658, doi:10.1038/ncb2718 (2013).

17 Demontis, F., Patel, V. K., Swindell, W. R. & Perrimon, N. Intertissue control of the nucleolus via a myokine-dependent longevity pathway. *Cell Rep* **7**, 1481-1494, doi:10.1016/j.celrep.2014.05.001 (2014).

18 Rai, M. *et al.* Proteasome stress in skeletal muscle mounts a long-range protective response that delays retinal and brain aging. *Cell metabolism* **33**, 1137-1154 e1139, doi:10.1016/j.cmet.2021.03.005 (2021).

19 Durieux, J., Wolff, S. & Dillin, A. The cell-non-autonomous nature of electron transport chain-mediated longevity. *Cell* **144**, 79-91, doi:10.1016/j.cell.2010.12.016 (2011).

20 Taylor, R. C. & Dillin, A. XBP-1 is a cell-nonautonomous regulator of stress resistance and longevity. *Cell* **153**, 1435-1447, doi:10.1016/j.cell.2013.05.042 (2013).

21 Demontis, F. & Perrimon, N. FOXO/4E-BP signaling in Drosophila muscles regulates organism-wide proteostasis during aging. *Cell* **143**, 813-825, doi:10.1016/j.cell.2010.10.007 (2010).
22 van Oosten-Hawle, P., Porter, R. S. & Morimoto, R. I. Regulation of organismal proteostasis by transcellular chaperone signaling. *Cell* **153**, 1366-1378, doi:10.1016/j.cell.2013.05.015 (2013).
23 Villeda, S. A. *et al.* The ageing systemic milieu negatively regulates neurogenesis and cognitive function. *Nature* **477**, 90-94, doi:10.1038/nature10357 (2011).
24 Conboy, I. M. *et al.* Rejuvenation of aged progenitor cells by exposure to a young systemic environment. *Nature* **433**, 760-764, doi:10.1038/nature03260 (2005).
25 Castellano, J. M. *et al.* Human umbilical cord plasma proteins revitalize hippocampal function in aged mice. *Nature* **544**, 488-492, doi:10.1038/nature22067 (2017).
26 Schaum, N. *et al.* Ageing hallmarks exhibit organ-specific temporal signatures. *Nature* **583**, 596-602, doi:10.1038/s41586-020-2499-y (2020).
27 Villeda, S. A. *et al.* Young blood reverses age-related impairments in cognitive function and synaptic plasticity in mice. *Nat Med* **20**, 659-663, doi:10.1038/nm.3569 (2014).
28 De Miguel, Z. *et al.* Exercise plasma boosts memory and dampens brain inflammation via clusterin. *Nature*, doi:10.1038/s41586-021-04183-x (2021).
29 Horowitz, A. M. *et al.* Blood factors transfer beneficial effects of exercise on neurogenesis and cognition to the aged brain. *Science* **369**, 167-173, doi:10.1126/science.aaw2622 (2020).
30 Ozek, C., Krolewski, R. C., Buchanan, S. M. & Rubin, L. L. Growth Differentiation Factor 11 treatment leads to neuronal and vascular improvements in the hippocampus of aged mice. *Sci Rep* **8**, 17293, doi:10.1038/s41598-018-35716-6 (2018).
31 Wrann, C. D. *et al.* Exercise induces hippocampal BDNF through a PGC-1α/FNDC5 pathway. *Cell Metab* **18**, 649-659, doi:10.1016/j.cmet.2013.09.008 (2013).
32 Islam, M. R. *et al.* Exercise hormone irisin is a critical regulator of cognitive function. *Nat Metab* **3**, 1058-1070, doi:10.1038/s42255-021-00438-z (2021).
33 Moon, H. Y. *et al.* Running-Induced Systemic Cathepsin B Secretion Is Associated with Memory Function. *Cell Metab* **24**, 332-340, doi:10.1016/j.cmet.2016.05.025 (2016).
34 White, P. J. *et al.* Protectin DX alleviates insulin resistance by activating a myokine-liver glucoregulatory axis. *Nature Medicine* **20**, 664-669, doi:10.1038/nm.3549 (2014).
35 Quinn, L. S., Anderson, B. G., Strait-Bodey, L., Stroud, A. M. & Argilés, J. M. Oversecretion of interleukin-15 from skeletal muscle reduces adiposity. *American Journal of Physiology-Endocrinology and Metabolism* **296**, E191-E202 (2009).
36 Boyle, P. A., Buchman, A. S., Wilson, R. S., Leurgans, S. E. & Bennett, D. A. Association of muscle strength with the risk of Alzheimer disease and the rate of cognitive decline in community-dwelling older persons. *Arch Neurol* **66**, 1339-1344, doi:10.1001/archneurol.2009.240 (2009).
37 Kim, J. *et al.* Association of muscle and visceral adipose tissues with the probability of Alzheimer's disease in healthy subjects. *Sci Rep* **9**, 949, doi:10.1038/s41598-018-37244-9 (2019).
38 Lourenco, M. V. *et al.* Exercise-linked FNDC5/irisin rescues synaptic plasticity and memory defects in Alzheimer's models. *Nat Med* **25**, 165-175, doi:10.1038/s41591-018-0275-4 (2019).
39 Gupta, R., Khan, R. & Cortes, C. J. Forgot to Exercise? Exercise Derived Circulating Myokines in Alzheimer's Disease: A Perspective. *Front Neurol* **12**, 649452, doi:10.3389/fneur.2021.649452 (2021).
40 Cortes, C. J. *et al.* Polyglutamine-expanded androgen receptor interferes with TFEB to elicit autophagy defects in SBMA. *Nat Neurosci* **17**, 1180-1189, doi:10.1038/nn.3787 (2014).
41 Cortes, C. J. & La Spada, A. R. Motor neuron degeneration in spinal and Bulbar Muscular Atrophy is a skeletal muscle-driven process: Relevance to therapy development and implications for related motor neuron diseases. *Rare Dis* **2**, e962402, doi:10.4161/2167549X.2014.962402 (2014).

42 Cortes, C. J. *et al.* Muscle expression of mutant androgen receptor accounts for systemic and motor neuron disease phenotypes in spinal and bulbar muscular atrophy. *Neuron* **82**, 295-307, doi:10.1016/j.neuron.2014.03.001 (2014).
43 Settembre, C. *et al.* TFEB links autophagy to lysosomal biogenesis. *Science* **332**, 1429-1433, doi:10.1126/science.1204592 (2011).
44 Palmieri, M. *et al.* Characterization of the CLEAR network reveals an integrated control of cellular clearance pathways. *Human molecular genetics* **20**, 3852-3866, doi:ddr306 [pii]

10.1093/hmg/ddr306 (2011).
45 Sardiello, M. *et al.* A gene network regulating lysosomal biogenesis and function. *Science* **325**, 473-477, doi:1174447 [pii]

10.1126/science.1174447 (2009).
46 Morgan, T. E. *et al.* The mosaic of brain glial hyperactivity during normal ageing and its attenuation by food restriction. *Neuroscience* **89**, 687-699, doi:10.1016/s0306-4522(98)00334-0 (1999).
47 van Praag, H., Shubert, T., Zhao, C. & Gage, F. H. Exercise enhances learning and hippocampal neurogenesis in aged mice. *J Neurosci* **25**, 8680-8685, doi:10.1523/jneurosci.1731-05.2005 (2005).
48 Zhu, H., Guo, Q. & Mattson, M. P. Dietary restriction protects hippocampal neurons against the death-promoting action of a presenilin-1 mutation. *Brain Res* **842**, 224-229, doi:10.1016/s0006-8993(99)01827-2 (1999).
49 Duan, W. & Mattson, M. P. Dietary restriction and 2-deoxyglucose administration improve behavioral outcome and reduce degeneration of dopaminergic neurons in models of Parkinson's disease. *J Neurosci Res* **57**, 195-206, doi:10.1002/(SICI)1097-4547(19990715)57:2<195::AID-JNR5>3.0.CO;2-P (1999).
50 Choi, S. H. *et al.* Combined adult neurogenesis and BDNF mimic exercise effects on cognition in an Alzheimer's mouse model. *Science* **361**, doi:10.1126/science.aan8821 (2018).
51 Leu, M. *et al.* Erbb2 regulates neuromuscular synapse formation and is essential for muscle spindle development. *Development* **130**, 2291-2301 (2003).
52 Decressac, M. *et al.* TFEB-mediated autophagy rescues midbrain dopamine neurons from alpha-synuclein toxicity. *Proceedings of the National Academy of Sciences of the United States of America* **110**, E1817-1826, doi:10.1073/pnas.1305623110 (2013).
53 Spampanato, C. *et al.* Transcription factor EB (TFEB) is a new therapeutic target for Pompe disease. *EMBO Mol Med* **5**, 691-706, doi:10.1002/emmm.201202176 (2013).
54 Klionsky, D. J. *et al.* Guidelines for the use and interpretation of assays for monitoring autophagy (3rd edition). *Autophagy* **12**, 1-222, doi:10.1080/15548627.2015.1100356 (2016).
55 Jiao, J. & Demontis, F. Skeletal muscle autophagy and its role in sarcopenia and organismal aging. *Curr Opin Pharmacol* **34**, 1-6, doi:10.1016/j.coph.2017.03.009 (2017).
56 Richardson, N. E. *et al.* Lifelong restriction of dietary branched-chain amino acids has sex-specific benefits for frailty and lifespan in mice. *Nat Aging* **1**, 73-86, doi:10.1038/s43587-020-00006-2 (2021).
57 Szklarczyk, D. *et al.* The STRING database in 2021: customizable protein-protein networks, and functional characterization of user-uploaded gene/measurement sets. *Nucleic Acids Res* **49**, D605-D612, doi:10.1093/nar/gkaa1074 (2021).
58 Cortazar, A. R., Oguiza, J. A., Aransay, A. M. & Lavin, J. L. VerSeDa: vertebrate secretome database. *Database (Oxford)* **2017**, doi:10.1093/database/baw171 (2017).
59 Lehallier, B. *et al.* Undulating changes in human plasma proteome profiles across the lifespan. *Nature Medicine* **25**, 1843-1850, doi:10.1038/s41591-019-0673-2 (2019).

60 Joly-Amado, A. *et al.* CCL2 Overexpression in the Brain Promotes Glial Activation and Accelerates Tau Pathology in a Mouse Model of Tauopathy. *Front Immunol* **11**, 997, doi:10.3389/fimmu.2020.00997 (2020).
61 Frakes, A. E. *et al.* Microglia induce motor neuron death via the classical NF-kappaB pathway in amyotrophic lateral sclerosis. *Neuron* **81**, 1009-1023, doi:10.1016/j.neuron.2014.01.013 (2014).
62 Islam, O., Gong, X., Rose-John, S. & Heese, K. Interleukin-6 and neural stem cells: more than gliogenesis. *Mol Biol Cell* **20**, 188-199, doi:10.1091/mbc.E08-05-0463 (2009).
63 Leibinger, M. *et al.* Interleukin-6 contributes to CNS axon regeneration upon inflammatory stimulation. *Cell Death Dis* **4**, e609, doi:10.1038/cddis.2013.126 (2013).
64 Yoshiyama, Y. *et al.* Synapse loss and microglial activation precede tangles in a P301S tauopathy mouse model. *Neuron* **53**, 337-351, doi:10.1016/j.neuron.2007.01.010 (2007).
65 Moloney, C. M., Lowe, V. J. & Murray, M. E. Visualization of neurofibrillary tangle maturity in Alzheimer's disease: A clinicopathologic perspective for biomarker research. *Alzheimers Dement* **17**, 1554-1574, doi:10.1002/alz.12321 (2021).
66 Jurga, A. M., Paleczna, M. & Kuter, K. Z. Overview of General and Discriminating Markers of Differential Microglia Phenotypes. *Front Cell Neurosci* **14**, 198, doi:10.3389/fncel.2020.00198 (2020).
67 Rozovsky, I., Finch, C. E. & Morgan, T. E. Age-related activation of microglia and astrocytes: in vitro studies show persistent phenotypes of aging, increased proliferation, and resistance to down-regulation. *Neurobiol Aging* **19**, 97-103, doi:10.1016/s0197-4580(97)00169-3 (1998).
68 Godbout, J. P. *et al.* Exaggerated neuroinflammation and sickness behavior in aged mice following activation of the peripheral innate immune system. *FASEB J* **19**, 1329-1331, doi:10.1096/fj.05-3776fje (2005).
69 Sidoryk-Wegrzynowicz, M. *et al.* Astrocytes in mouse models of tauopathies acquire early deficits and lose neurosupportive functions. *Acta Neuropathol Commun* **5**, 89, doi:10.1186/s40478-017-0478-9 (2017).
70 Knopman, D. S. *et al.* Alzheimer disease. *Nat Rev Dis Primers* **7**, 33, doi:10.1038/s41572-021-00269-y (2021).
71 Preuss, C. *et al.* A novel systems biology approach to evaluate mouse models of late-onset Alzheimer's disease. *Mol Neurodegener* **15**, 67, doi:10.1186/s13024-020-00412-5 (2020).
72 Chai K, L. J., Zhang X, Gu H, Cao P, Ye W, Tang H, Liu J, Chen S, Wan F, Liu GL, Shen D. ARHGDIB Plays a Novel Role in the Braak Stages of Alzheimer's Diseases via the Immune Response Mediated by Microglia

Pre-print: Research Square, doi:10.21203/rs.3.rs-474315/v1 (2021).
73 Moon, S. W. *et al.* Structural Neuroimaging Genetics Interactions in Alzheimer's Disease. *J Alzheimers Dis* **48**, 1051-1063, doi:10.3233/JAD-150335 (2015).
74 Wohlgemuth, S. E., Seo, A. Y., Marzetti, E., Lees, H. A. & Leeuwenburgh, C. Skeletal muscle autophagy and apoptosis during aging: effects of calorie restriction and life-long exercise. *Experimental gerontology* **45**, 138-148, doi:10.1016/j.exger.2009.11.002 (2010).
75 Grumati, P. *et al.* Autophagy is defective in collagen VI muscular dystrophies, and its reactivation rescues myofiber degeneration. *Nat Med* **16**, 1313-1320, doi:10.1038/nm.2247 (2010).
76 He, C., Sumpter, R., Jr. & Levine, B. Exercise induces autophagy in peripheral tissues and in the brain. *Autophagy* **8**, 1548-1551, doi:10.4161/auto.21327 (2012).
77 Masiero, E. *et al.* Autophagy is required to maintain muscle mass. *Cell Metab* **10**, 507-515, doi:10.1016/j.cmet.2009.10.008 (2009).

78 Raben, N. *et al.* Suppression of autophagy in skeletal muscle uncovers the accumulation of ubiquitinated proteins and their potential role in muscle damage in Pompe disease. *Human molecular genetics* **17**, 3897-3908, doi:10.1093/hmg/ddn292 (2008).
79 Vainshtein, A., Grumati, P., Sandri, M. & Bonaldo, P. Skeletal muscle, autophagy, and physical activity: the menage a trois of metabolic regulation in health and disease. *J Mol Med (Berl)* **92**, 127-137, doi:10.1007/s00109-013-1096-z (2014).
80 Bostrom, P. *et al.* A PGC1-alpha-dependent myokine that drives brown-fat-like development of white fat and thermogenesis. *Nature* **481**, 463-468, doi:10.1038/nature10777 (2012).
81 Otaka, N. *et al.* Myonectin Is an Exercise-Induced Myokine That Protects the Heart From Ischemia-Reperfusion Injury. *Circ Res* **123**, 1326-1338, doi:10.1161/CIRCRESAHA.118.313777 (2018).
82 Ximerakis, M. *et al.* Single-cell transcriptomic profiling of the aging mouse brain. *Nat Neurosci* **22**, 1696-1708, doi:10.1038/s41593-019-0491-3 (2019).
83 Baughman, H. E. R., Clouser, A. F., Klevit, R. E. & Nath, A. HspB1 and Hsc70 chaperones engage distinct tau species and have different inhibitory effects on amyloid formation. *J Biol Chem* **293**, 2687-2700, doi:10.1074/jbc.M117.803411 (2018).
84 Thompson, A. D. *et al.* Analysis of the tau-associated proteome reveals that exchange of Hsp70 for Hsp90 is involved in tau degradation. *ACS Chem Biol* **7**, 1677-1686, doi:10.1021/cb3002599 (2012).
85 Marina, N. *et al.* Astrocytes monitor cerebral perfusion and control systemic circulation to maintain brain blood flow. *Nat Commun* **11**, 131, doi:10.1038/s41467-019-13956-y (2020).
86 Searle, B. C. *et al.* Chromatogram libraries improve peptide detection and quantification by data independent acquisition mass spectrometry. *Nat Commun* **9**, 5128, doi:10.1038/s41467-018-07454-w (2018).
87 Pino, L. K., Just, S. C., MacCoss, M. J. & Searle, B. C. Acquiring and Analyzing Data Independent Acquisition Proteomics Experiments without Spectrum Libraries. *Mol Cell Proteomics* **19**, 1088-1103, doi:10.1074/mcp.P119.001913 (2020).
88 Amodei, D. *et al.* Improving Precursor Selectivity in Data-Independent Acquisition Using Overlapping Windows. *J Am Soc Mass Spectrom* **30**, 669-684, doi:10.1007/s13361-018-2122-8 (2019).
89 Kall, L., Canterbury, J. D., Weston, J., Noble, W. S. & MacCoss, M. J. Semi-supervised learning for peptide identification from shotgun proteomics datasets. *Nat Methods* **4**, 923-925, doi:10.1038/nmeth1113 (2007).
90 Ritchie, M. E. *et al.* limma powers differential expression analyses for RNA-sequencing and microarray studies. *Nucleic Acids Res* **43**, e47, doi:10.1093/nar/gkv007 (2015).
91 Smyth, G. K. Linear models and empirical bayes methods for assessing differential expression in microarray experiments. *Stat Appl Genet Mol Biol* **3**, Article3, doi:10.2202/1544-6115.1027 (2004).
92 Shannon, P. *et al.* Cytoscape: a software environment for integrated models of biomolecular interaction networks. *Genome Res* **13**, 2498-2504, doi:10.1101/gr.1239303 (2003).
93 Guyenet, S. J. *et al.* A simple composite phenotype scoring system for evaluating mouse models of cerebellar ataxia. *J Vis Exp*, doi:10.3791/1787 (2010).

Figure 1: cTFEB;HSACre mice have increased skeletal muscle proteostasis

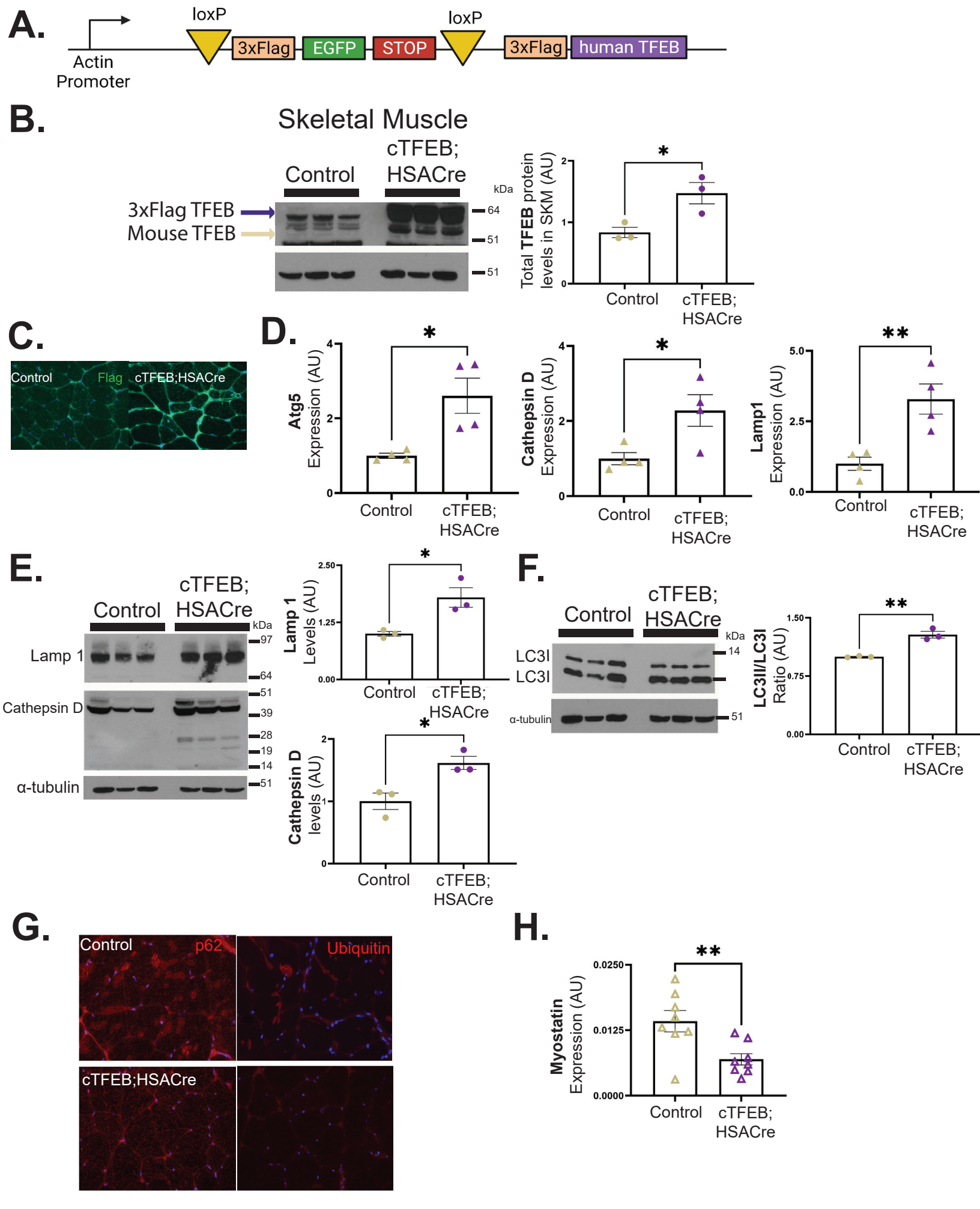

Figure 2: Proteomics analysis identifies increased proteostasis in TFEB-overexpressing skeletal muscle

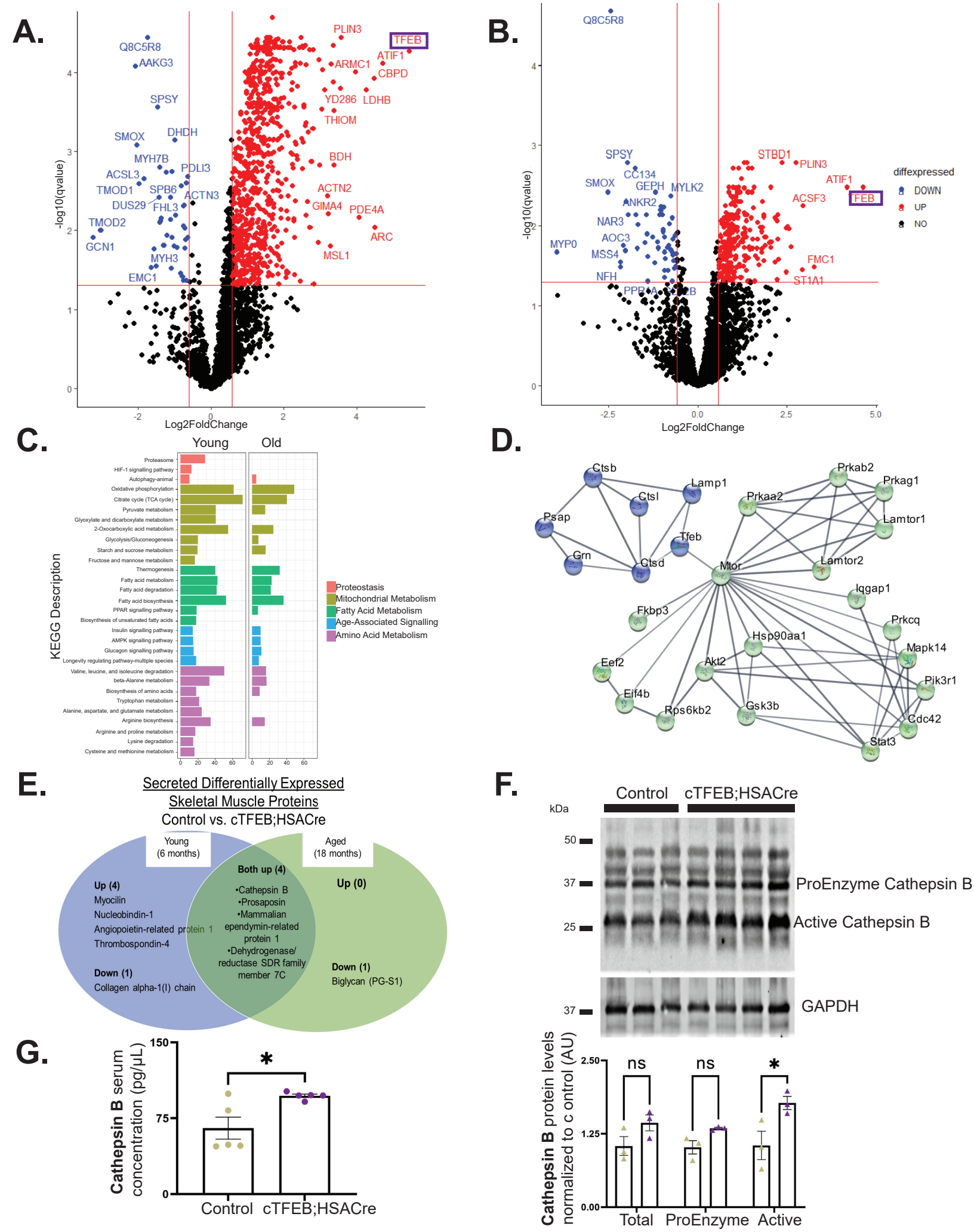

Figure 3: Peripheral over-expression of TFEB decreases neuroinflammation, lipofuscin accumulation, and rescues behavior in aged mice

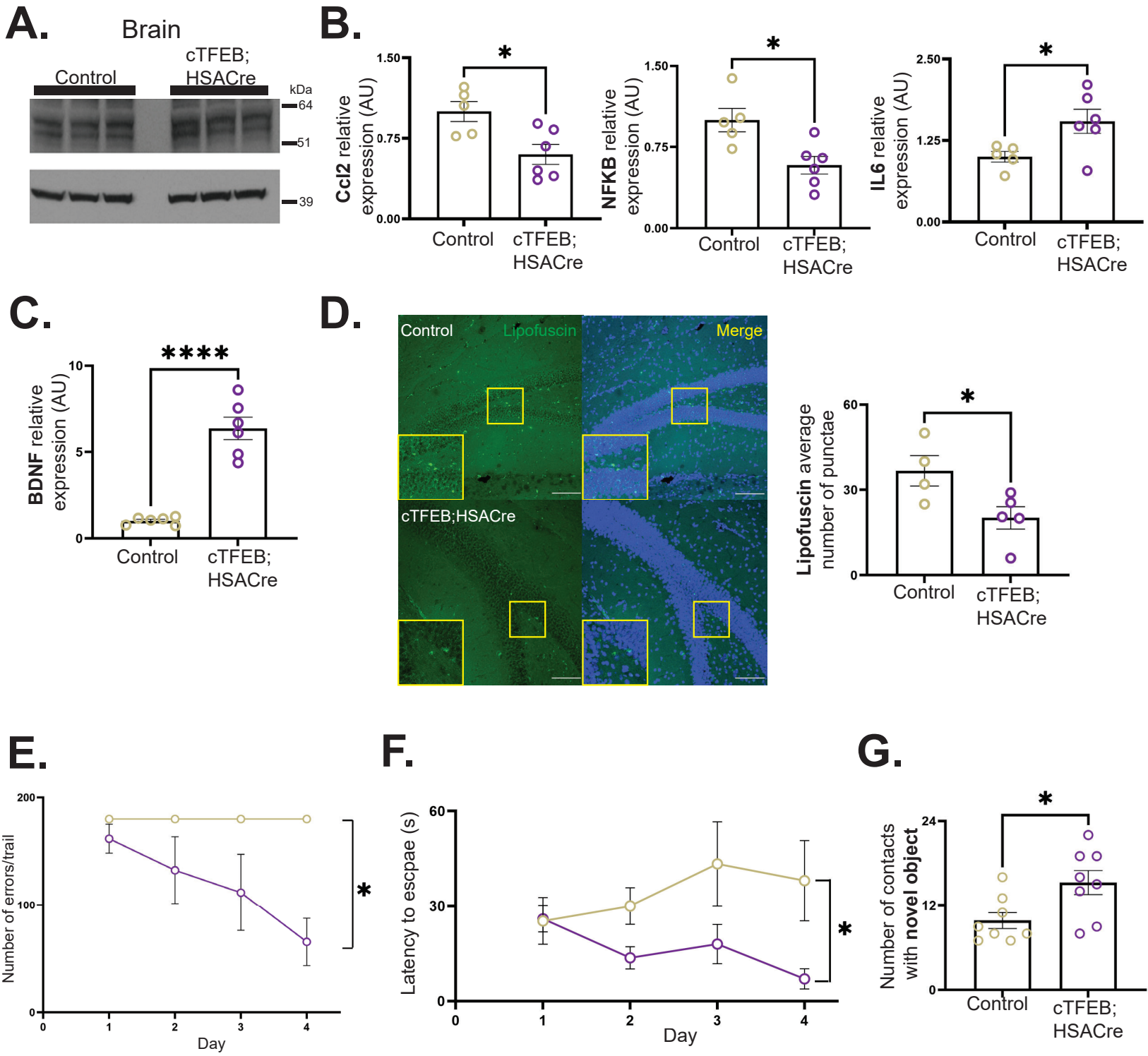

Figure 4: Neurotrophic transcriptome changes in the hippocampi of cTFEB;HSACre mice.

A.

Expression changes in Young Female cTFEB;HSACre

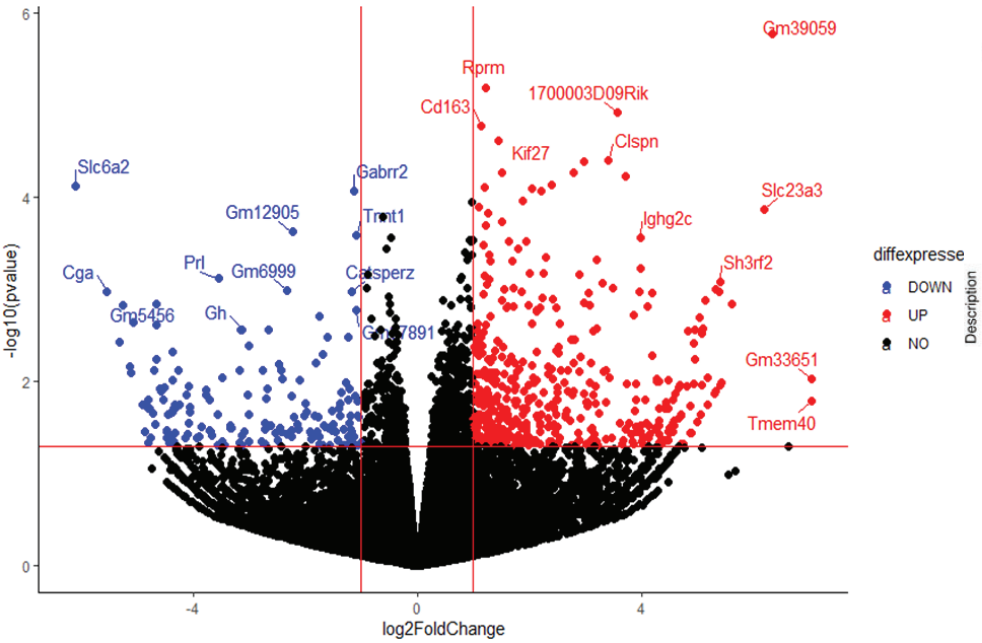

B.

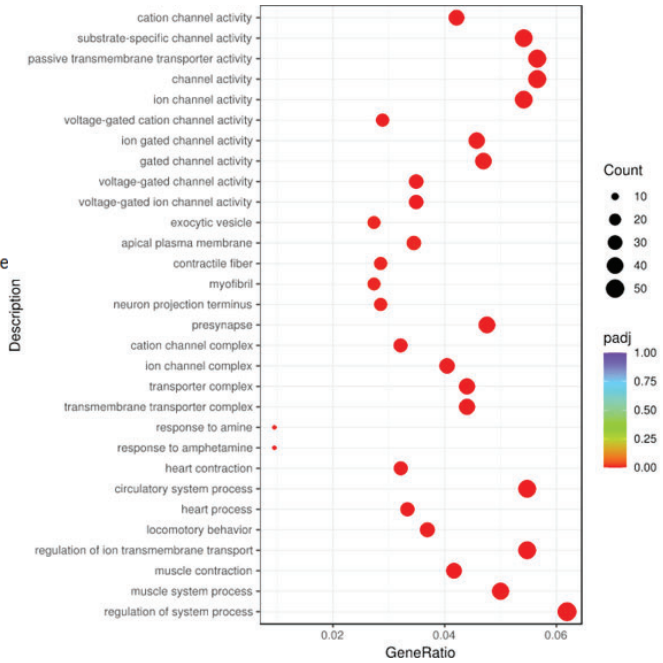

C.

Expression changes in Old Female cTFEB;HSACre

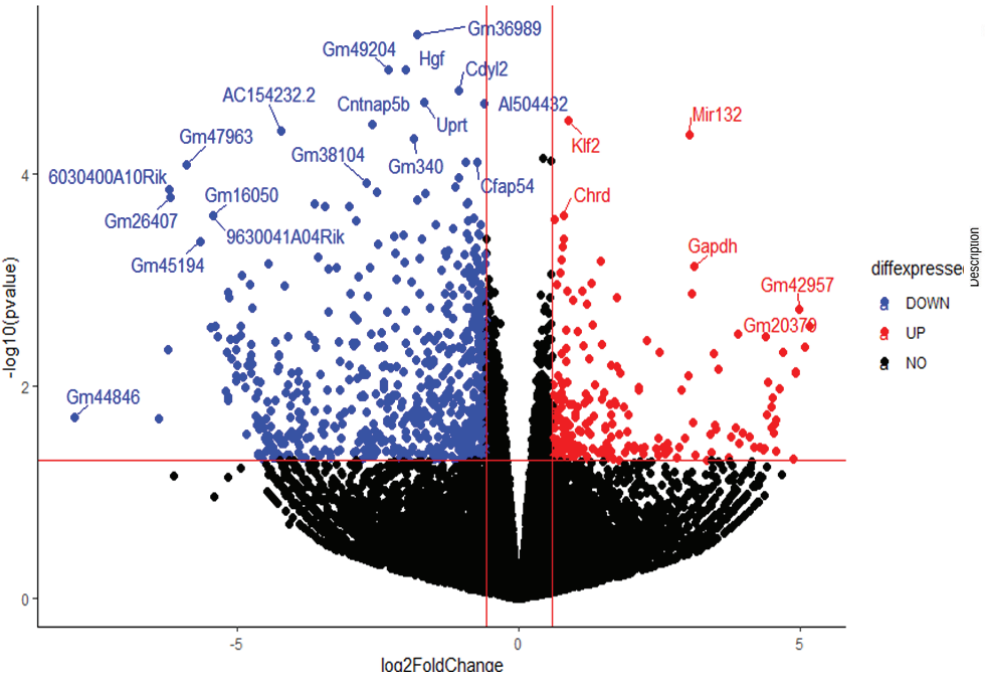

D.

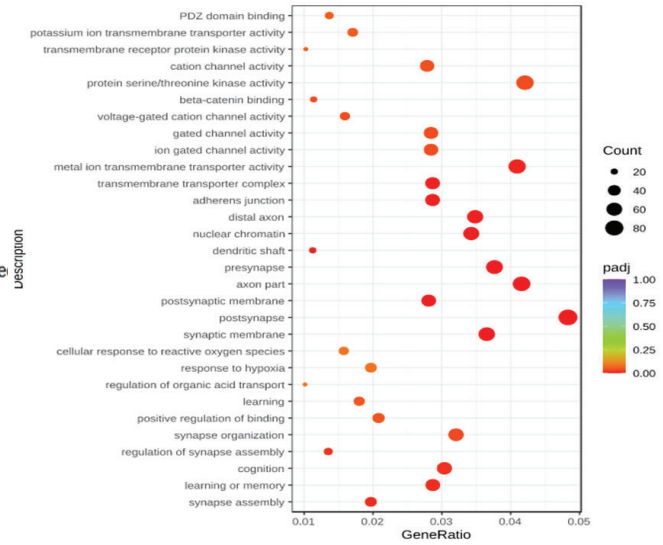
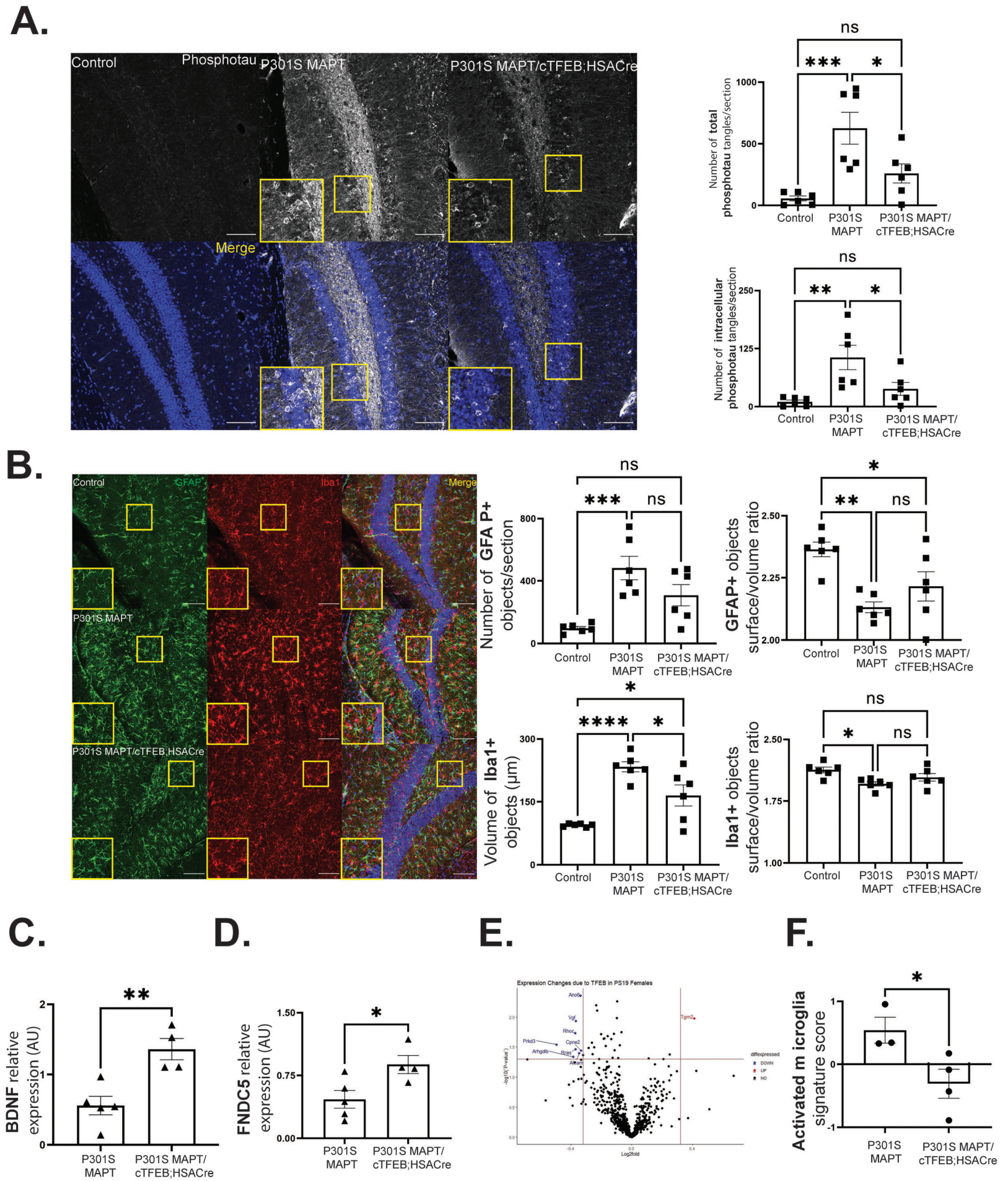
Figure 5: Enhanced skeletal muscle proteostasis rescues mouse model of tau pathology